Hindawi
Geofluids
Volume 2021, Article ID 3980170, 13 pages
https://doi.org/10.1155/2021/3980170

Research Article

Role Played by Oil Emplacement in Controlling Pore Network Evolution of Tight Sandstones

Huifang Hu,[1,2] Yang Ju,[1] Chenyang Zhao,[3] Miaozhi Jing,[4] Liang Sun,[5] Wei Sun,[6] Dengke Liu,[7] Lin Yang,[8] Yue Jing,[7] and Guoqiang Huang[7]

[1]*State Key Laboratory of Coal Resources and Safe Mining, China University of Mining and Technology, Beijing 100083, China*
[2]*Exploration and Development Research Institute, Shengli Oilfield, SINOPEC, Dongying 257015, China*
[3]*Exploration and Development Research Institute, Changqing Oilfield Company, PetroChina, Xi'an 710018, China*
[4]*No. 1 Gas Production Plant, Changqing Oilfield Company, PetroChina, Xi'an 710018, China*
[5]*No. 11 Oil Production Plant, Changqing Oilfield Company, PetroChina, Qingyang 745000, China*
[6]*Department of Geology, Northwest University, Xi'an 710069, China*
[7]*School of Human Settlement and Civil Engineering, Xi'an Jiaotong University, Xi'an 710049, China*
[8]*CNPC Well Logging, Xi'an 710000, China*

Correspondence should be addressed to Yang Ju; juy@cumtb.edu.cn and Dengke Liu; liudengke02@126.com

Received 7 May 2021; Accepted 24 September 2021; Published 16 October 2021

Academic Editor: Sohrab Zendehboudi

Whether oil emplacement and diagenetic sequences provoke, deteriorate, or have no effect on pore network evolution, as implied by recent tests and theoretical analysis, are critical factors in forecasting hydrocarbon exploration and development potentials. Therefore, a systematic investigation on the effect of oil emplacement of tight sandstones is conducted to study the importance of this behavior on the pore evolution path. This study evaluated the role played by oil emplacement and diagenesis in the pore network evolution of Upper Triassic tight sandstones in the Ordos Basin. To help provide a comprehensive understanding, we have used a multidisciplinary method including physical properties, casting thin section, scanning electron microscope, X-ray diffraction, fluorometric, and inclusion analysis. The results demonstrate that the sandstones could be divided into four groups based on new criteria: calcareous sandstone, high soft component sandstone, low soft component sandstone with continual oil emplacement, and low soft component sandstone with intermittent oil emplacement. The physical properties of those types of sandstones were gradually reduced. Quartz cement captured hydrocarbon, carbonate captured hydrocarbon, free hydrocarbon, and adsorbed hydrocarbon were the four main kinds of hydrocarbons. The maturity of those sandstones was decreased progressively, indicating that the formation time of those hydrocarbons was favorable to maturity. Four stages of oil emplacement happened, and large-scale emplacement mainly occurred in the late Jurassic and early Craterous. The evidence demonstrated that tight sandstones' high porosity could be attributed to positive diagenetic contributions with a complex interplay of chemical compaction, early formed clays, and large-scale oil emplacement. This work would provide new sights for a better understanding of the tight oil accumulation modes, and the findings could be applied in the hydrocarbon exploration and development field.

1. Introduction

The exploration and development method in Ordos Basin, China, has varied many times over the past few years [1]. That is because of the gradual shift of the targets from conventional reservoirs to unconventional reservoirs [2]. A tight sandstone reservoir, one of the typical unconventional reservoirs, contains pores and throats ranging from $<1\,\mu$m up to macroscale and has complex pore-throat structures [3–7]. The Upper Triassic lithologies within the basin can predominantly be addressed as a tight reservoir [8, 9]. Determination of pore-throat structure is critical for the potential reserve calculation. Pore network evolution is one of the most significant research points in pore structure systems.

It can reflect petrophysical properties, oil and gas filling, migration, and accumulation in tight sandstones [10, 11]. Studies on the pore network evolution in porous geomaterials are crucial to hydrocarbon exploration and development. It is widely believed that the evolution path of the pore network evolution is strongly controlled by the diagenesis and tectonic movement [12–14]. As the tectonic movement went on, the internal and external pressure within the reservoir would change, led to the variation of confining pressure, and caused the pore structure change. How diagenesis impacts the pore network evolution has widely been studied; compaction, dissolution, and cementation are the three typical diagenesis, and different kinds of diagenesis have different functions [15–18].

Oil emplacement is another essential factor in pore network evolution compared to diagenesis and tectonic movement [19]. Two types of models explain the relationship between oil emplacement and pore network evolution. The first one is the "oil-inhibits-diagenesis" model, which suggests that oil emplacement would prevent diagenetic minerals' formation from preserving the pore spaces [20]. Another is the "oil-does-not-inhibit-diagenesis" model, which demonstrates that the oil has no impact on diagenetic evolution. Then, the porosity would decrease obviously during the diagenetic path [20]. The thickness and distribution of the source rock of the Upper Triassic reservoir in the basin are widely developed, makes its importance even more apparent [21, 22]. However, much work has been undertaken to study the coupling relationship between oil emplacement and pore network evolution. How oil influence the formation of the diagenetic mineral remains a myth. Therefore, various experimental approaches have been adopted to cast further light on whether oil emplacement impacts the pore network evolution.

This study is aimed at understanding the occurrence state of the oil and the effect of oil emplacement on pore network evolution in tight sandstones. To achieve this, sandstone samples were subjected to physical properties, casting thin section, scanning electron microscopy, X-ray diffraction, fluorometric analysis, and inclusion analysis. The main questions addressed by this research are as follows:

(1) Are there any new rock classification types that could suit the pore network evolution and oil emplacement study?

(2) How many stages can the oil emplacement be divided into?

(3) How do different stages of oil emplacement impact on the pore network evolution?

The interactive flowchart that shows the procedure of the research is as follows (Figure 1).

2. Methodology

2.1. Geological Setting. The Ordos Basin is a large petroliferous sedimentary basin in northwestern China, covering about 370,000 km^2 (Figure 2(a)) [17]. It is surrounded by the Yin Mountain to the north, Long Mountain to the south, Helan Mountain to the west, and LvLiang Mountain to the east. The basin is built upon a cratonic basement, and it has less tectonic movement [23]. Sandstones, carbonates, and shales dominate in the Ordos Basin [24]. The research objects are from the Chang 8 (C8) sandstones of the Upper Triassic strata, and the samples are located in the southwestern of the Ordos Basin (Figure 2(b)).

2.2. Physical Properties. Porosity and permeability are the two main types of physical properties. In this research, helium-based porosity and nitrogen-based permeability were performed on 2.5×2.5 cm core samples using an FYK-I apparatus. Before the tests, the samples were oil washed and dried at a temperature over 110°C. Inject the helium into the reference chamber. When the pressure becomes stable, document the pressure of the reference and core chamber. Open the junction valve, let the pressure in those two chambers becomes stable and document the pressure value. Finally, use Boyle's law to determine the chamber volumes. The calculation methods of the core sample volumes were similar to that of chamber volumes, and core volumes and pore volumes could determine the porosity. As for the permeability calculation, the cores were put into the holder initially, then pressurized to 10 MPa. After that, inject nitrogen and document pore pressure. Open the junction valve, record the differential pressure and time in every 1 psi, and calculate the permeability based on the pulse equation.

2.3. Casting Thin Section. The casting thin sections were stained by mixed solution (60% ARS solution: 2 mL concentrated hydrochloric acid, 998 mL distilled water, and 1 g alizarin red S; 40% PF solution: 1.5 mL concentrated hydrochloric acid, 98.5 mL distilled water, and 2 g potassium ferricyanide) and cemented by red epoxy resin. A Nikon LV100POL microscope was employed under transmitted light using plain polarized light. The main types of pores were examined, and the proportion of grain mineral, cement, and matrix was calculated by counting 300 points for each sample.

2.4. Scanning Electron Microscopy. The GeminiSEM 500 scanning electron microscope produced by ZEISS Company was selected for the analysis. An accelerating voltage and a current emission were set as 15 kV and 100 pA, respectively. The samples were first cut to $8 \times 8 \times 5$ mm and washed by an oil displacement agent. Then, all samples were put into the drying oven at 105°C. To avoid the electron charging effect, all samples were coated with carbon thick of 10-20 nm before the tests. The experiments were performed under the temperature of 25°C and humidity of 40%.

2.5. X-Ray Diffraction. For mineral determination quantitatively, the X'Pert PRO energy dispersive X-ray spectrometer was used. All the samples were dried at the temperature of 60°C and crushed under 120 mesh after oil-washed. Put the powder into the groove and made the aimed test surface rough. Selected the CuKα radiation, and the angle between emission and radiation slit was set as 1°. The

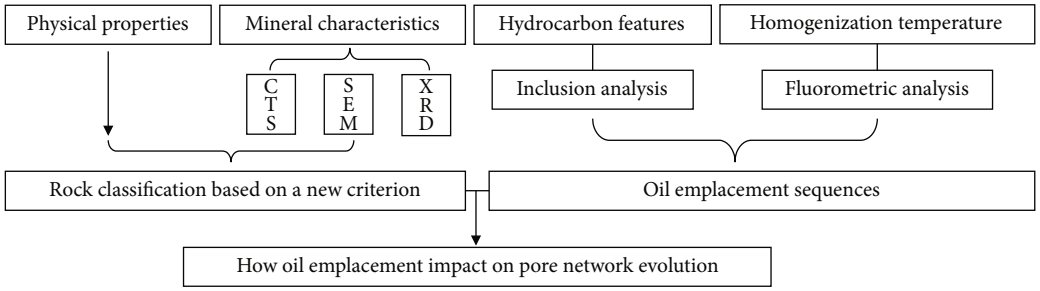

Figure 1: The interactive flowchart of the research.

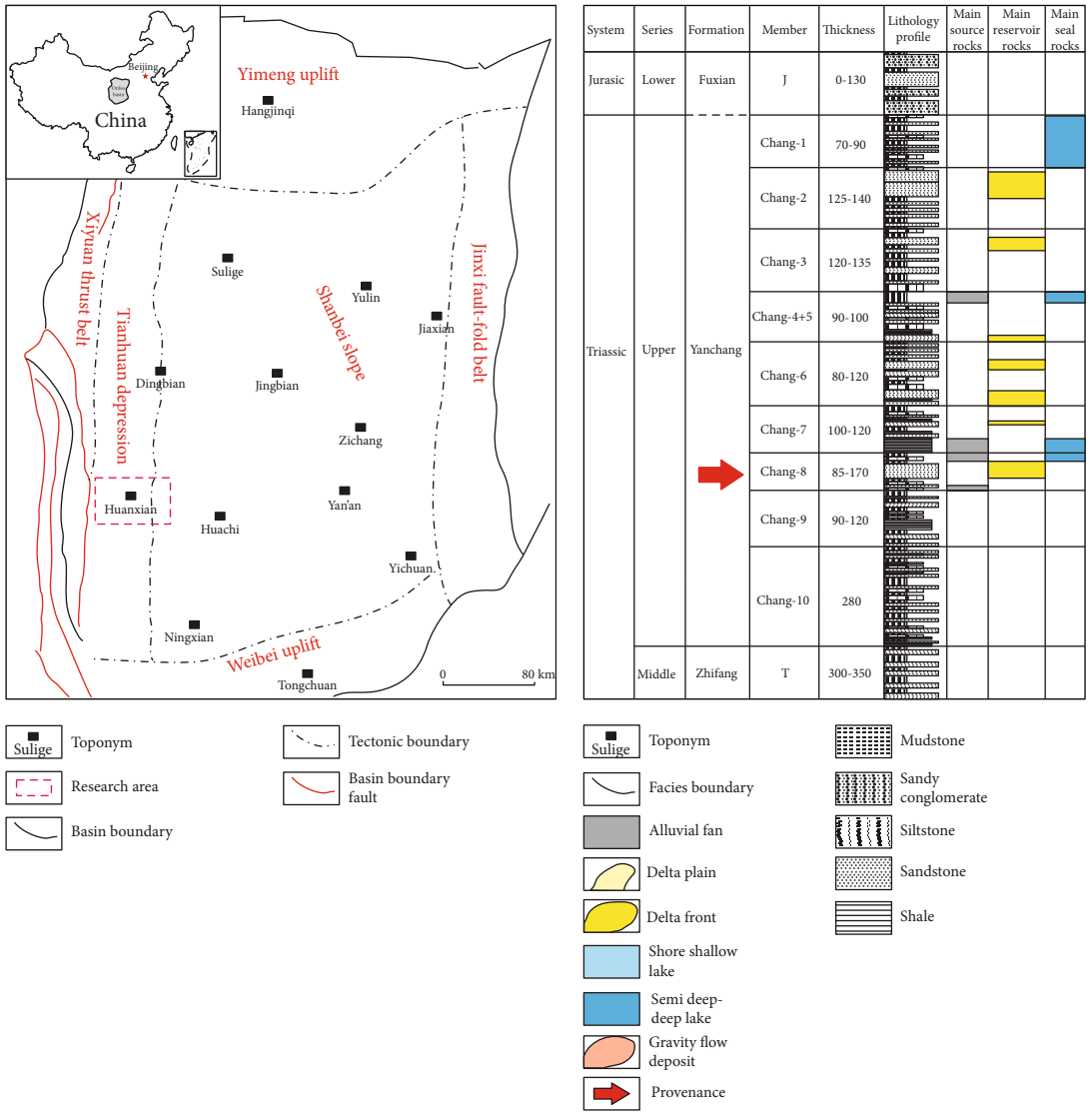

Figure 2: (a) Study area; (b) stratigraphic column and locations of samples. Revised from Liu et al. [22].

scanning velocity and sampling step width, both of them were under the condition of 2θ (5°-45°), were selected as 2°/min and 0.02, respectively. Measured the integral intensity of diffraction peak and calculated the content of minerals quantitatively.

2.6. Fluorometric Analysis. The samples were observed under UV light for fluorometric analysis. Leica MZ10F reflected-light microscope was selected as the instrument. The Adobe Photoshop CS3 captured the photographs, and the filter fluorometer was used to determine the triplicate plates.

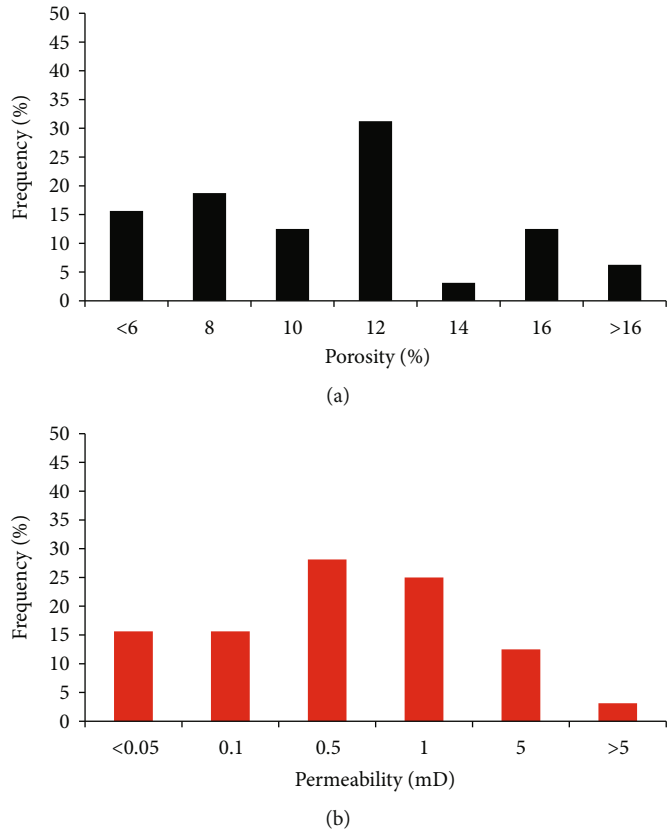

Figure 3: The (a) porosities and (b) permeabilities of C8 sandstones.

2.7. Inclusion Analysis. The homogenization temperature of fluid inclusions in a certain horizon represents the temperature of the strata in the capture period. Brine inclusions coexisting with hydrocarbon inclusions are selected for this temperature measurement, and the measured temperature represents the temperature of strata in different diagenetic evolution stages. The samples were first polished as thin sections and picked up some typical fluid inclusions. All picked inclusions recorded the types, shape, radius, distributions, and gas ratio. The THMS600 cooling-heating stage was selected to exam the temperature with the temperature from -180 to 600°C. Before the samples were put into the apparatus, the standard melting point of the reagent was selected for cooling-heating stage correction. The samples were repeatedly warmed and cooled, and some significant parameters, such as homogenization temperature, were determined.

3. Results

3.1. Physical Properties of the Tight Sandstones. The porosities and permeabilities of the C8 Formation sandstones are illustrated in Figure 3 and Table S1. The cored samples have porosities of 3.7-19.2%, with an average of 10.14%. The sandstones have permeabilities of 0.013-5.890 mD, with an average of 0.720 mD. The data showed that C8 sandstones are typical tight sandstones with low porosity and low permeability.

3.2. Mineral Characteristics. The sandstones of the C8 Formation are pervasively clay minerals abundant, and the detailed data were demonstrated in Table S2. Feldspar, quartz, and rock fragment were identified based on thin-section observations, and the distribution of mica is rare, and they are volumetrically less than 6% (Figures 4(a)–4(c)). Kaolinite is the predominant clay mineral in C8 sandstones, followed by chlorite and illite, while I/S mixed layer was in trace amount (Figures 4(d)–4(f)).

3.3. Hydrocarbon Types and Their Geochemical Properties. In geological time, oil emplacement and diagenesis happened simultaneously [25–27]. Therefore, various kinds of hydrocarbons are remaining in the minerals or matrix pore space. In this part, we first used fluorometric analysis to determine the hydrocarbon types qualitatively. We then measured some geochemical parameters of different types, including compositions, odd-even carbon ratio of organic matter, and vitrinite reflectance. Finally, some geochemical properties of various hydrocarbons were analyzed, which produced the foundation for further study.

Fluorometric analysis was used for the qualitative recognition of hydrocarbons. In this research area, based on the distributions of the hydrocarbons, it can be grouped into four categories: ① quartz cement captured hydrocarbon, the oils are distributed within the intercrystalline pores of the quartz; ② carbonate captured hydrocarbon, the oils are captured when carbonate formed during diagenetic ages; ③

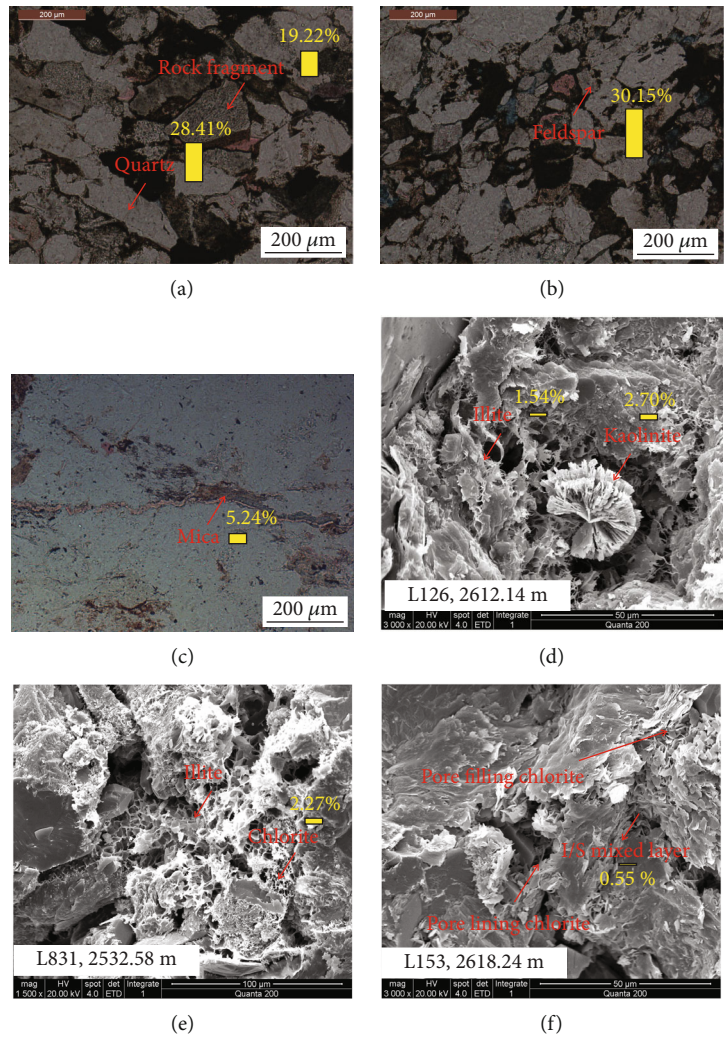

Figure 4: Types and proportions of different minerals.

free hydrocarbon, which distributed in the center of pores; and ④ adsorbed hydrocarbon, the occurrence of which could be divided into two main types: pore lining and corner lining styles (Figure 5).

Apart from that qualitative analysis, some geochemical properties were used for quantitative analysis. Figure 6 illustrates the compositions of different types of hydrocarbons. The figure shows that saturated hydrocarbon plays a dominant role in the free hydrocarbons, followed by aromatic hydrocarbons, while the other two were in trace amounts. Saturated, aromatic, and nonhydrocarbons occupied significant positions for the adsorbed hydrocarbon. Nonhydrocarbons and asphaltene are the predominant compositions for the captured hydrocarbons. The maturity of saturated, aromatic, nonhydrocarbons, and asphaltene has sorted the array in descending order. Therefore, based on the components of different hydrocarbons, the maturity could be determined: free, adsorbed, carbonate captured, and quartz cement captured hydrocarbons sorted from the largest to the smallest. The plot of odd-even carbon ratio of matter values to vitrinite reflectance also concluded similar results and behaviors: the decrease of odd-even carbon ratio of matter values and the increase of vitrinite reflectance reflect the increase of maturity. Hence, these results were corresponding to the aforementioned findings. Detailed data were demonstrated in Table S3.

3.4. Homogenization Temperature. Figure 7 illustrates the histogram of the inclusion homogenization temperature in the research area. The figure shows that the homogenization temperature ranged from 70 to 150°C and mainly concentrated in 90-130°C. The detailed data were demonstrated in Table S4.

4. Discussion

4.1. Rock Classification Based on a New Criterion. The classical sandstone classification, such as Folk's classification, was widely used in previous studies [28, 29]. These classifications are based on the percentage of quartz, feldspar, and rock fragments combined with the grain size and observations on casting thin sections to analyze the rock

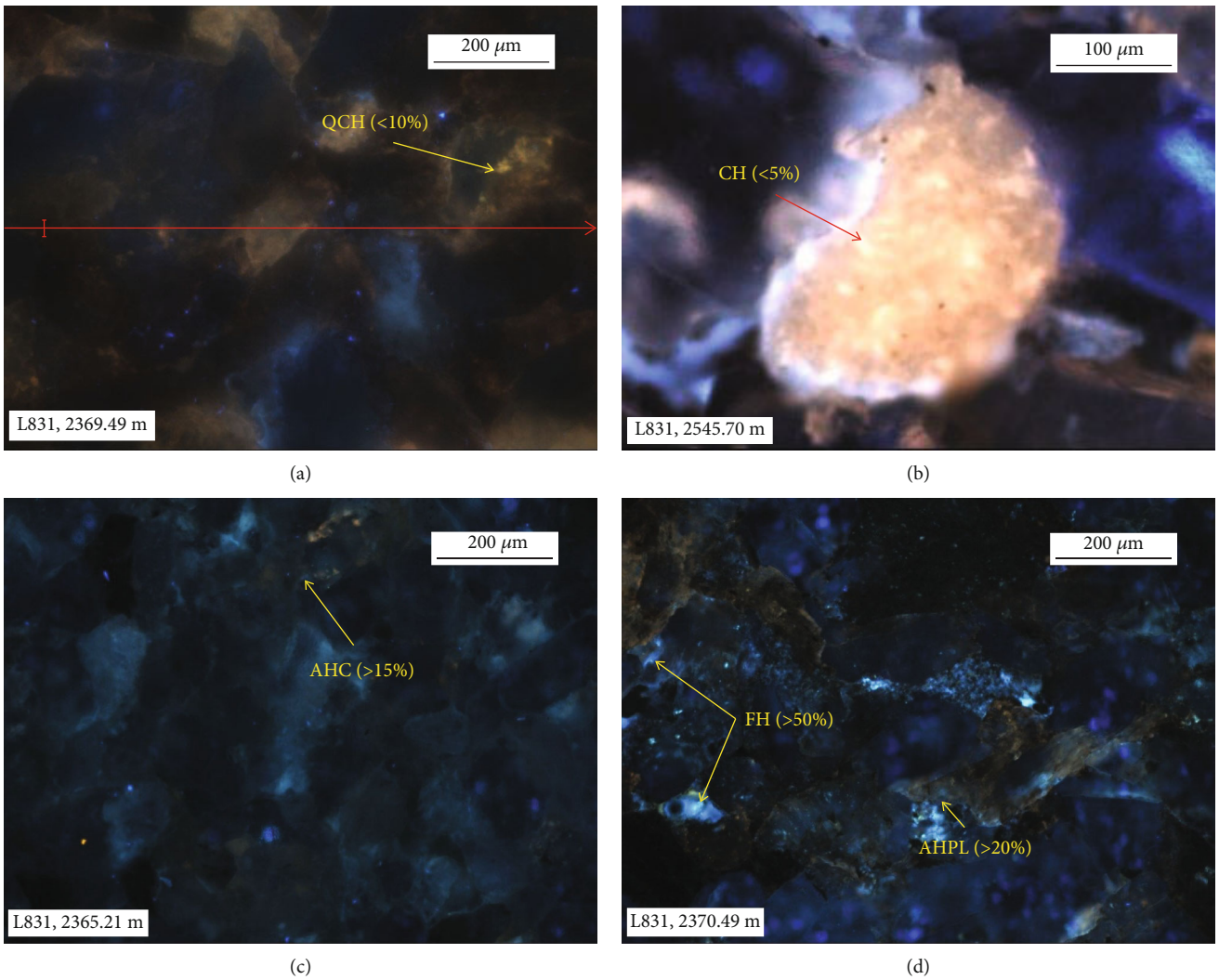

Figure 5: Crude oil fluorometric photograph scheme established for the study: (a) quartz cement captured hydrocarbon (QCH); (b) carbonate captured hydrocarbon (CH); (c) adsorbed hydrocarbon in the corner (AHC); (d) free hydrocarbon (FH) and adsorbed hydrocarbon in pore-lining style (AHPL).

compositions. Although the classical classifications could reflect the main types of sandstones, there are no good diagenetic process analysis methods. In this research, we proposed a new criterion for the sandstone classification. The triangle's composition was replaced by ① grain skeleton, which represents the rigid grain minerals, the abundance of which generally show weak compaction; ② soft component, which means the ductile mineral; and ③ calcite cement, the abundance of which usually represent early solid cementation. Based on this classification criterion, the samples could be divided into calcareous sandstone, high soft component sandstone, and low soft component sandstone. Hydrocarbon filling would dissolve the calcite minerals. Therefore, carbonate, the typical calcite mineral, could be a good indicator for further classification. The low soft component sandstone can be further divided into low soft component sandstone with continual oil emplacement and low soft component sandstone with intermittent oil emplacement. Therefore, four types of sandstones were determined in this research (Figure 8).

4.2. Physical Properties of Different Types of Sandstones. Figure 9 demonstrates the distributions of porosity and permeability and their relationships. Ten typical samples were selected from each group randomly. The results show good positive relationships between porosities and permeabilities for calcareous sandstone and low soft component sandstone with intermittent oil emplacement. For the other two groups, those parameters are independent.

Generally, porosity would have good relationships with permeability. The reasons caused these phenomena were explained in Figures 9(b) and 9(c). Strong compaction would make the soft component deformed for the high soft component sandstone; some seepage path formed, leading to high permeability while low porosity. For the low soft component sandstone with continual oil emplacement,

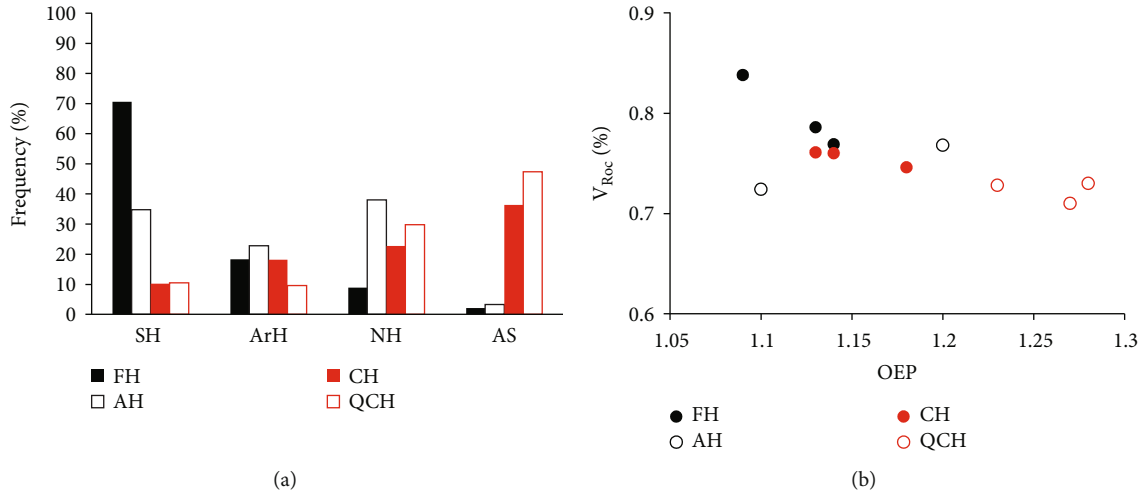

Figure 6: (a) Histogram of hydrocarbon distribution; (b) plot of odd-even carbon ratio of organic matter (OEP) values to vitrinite reflectance (R_o). FH: free hydrocarbon; AH: adsorbed hydrocarbon; CH: carbonate hydrocarbon; QCH: quartz cement hydrocarbon; SH: saturated hydrocarbon; ArH: aromatic hydrocarbon; NH: nonhydrocarbon; As: asphaltene.

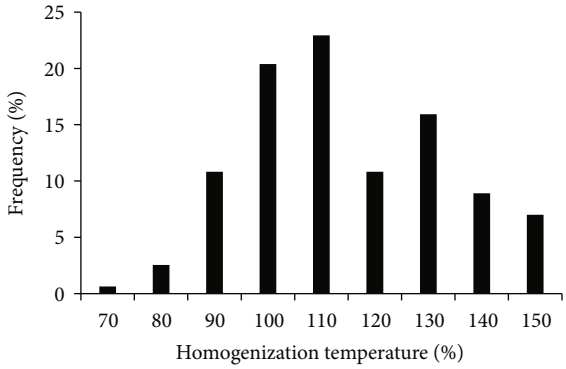

Figure 7: Histogram of homogenization temperature.

abundant hydrocarbon filling would make some Ca^{2+} related minerals dissolved, result in large pores. However, the dissolution parts were usually restrained from the specific minerals, making the effective seepage path hard to form, leading to low permeability.

4.3. Oil Emplacement Sequences. To determine the oil emplacement sequences, the geological time of the emplacement needs to be calculated first. Fluid inclusion could record the minerals' formation time, thus reflecting the emplacement time of the fluids that remained in the minerals. In this way, when we tested the temperatures of brine inclusions in the minerals, the temperatures of coformed oil inclusions could also be determined. Then, the oil emplacement corresponding temperature could be ascertained (Figure 7).

The homogenization temperatures from different captured minerals were tested. Figure 9(a) shows that the homogenization temperatures of calcareous sandstone, high soft component sandstone, low soft component sandstone with continual oil emplacement, and low soft component sandstone with intermittent oil emplacement were 53.5 ~ 118.3/83.6, 65.2 ~ 128.1/94.5, 70.6 ~ 131.7/100.9, and 100.1 ~ 149.6/124.3°C, respectively, demonstrating that the emplacement ages were getting newer and newer.

One dimension burial history modeling was established by Schlumberger's PetroMod (V2014.1) software to analyze the burial and thermal history of the strata. A typical well was selected to represent the research area (Figure 10). The model was established using the present-day well strata, bottom hole temperature, geotectonic, and terrestrial heat flow data. The homogenization temperatures measured in this research were used for the burial and temperature correction. Based on the homogenization temperature and the burial modeling, the emplacement sequences were determined: the first emplacement was happened in the early Jurassic, followed by the second emplacement in late Jurassic, then in the early Cretaceous, third round emplacement began, and the last round finished in late Cretaceous.

4.4. The Coupling Relationships between Diagenesis and Oil Emplacement. The depth of Chang 8 members in the study area is between 1900 and 2600 m. $R = 3$ Reichweite illite smectite mixed layer ratio is abundant. The homogenization temperature of inclusions is between 70 and 160°C, mainly in the late B stage of the middle diagenesis. The judgment of diagenetic sequences was based on the following criteria: ① compaction rates were positive to the burial speed; ② early formed interstitial minerals were adjacent to the pore wall; ③ late formed ones were grew in the middle of the pores; and ④ dissolution age was closely related to the oil emplacement time (Figures 10 and 11). Therefore, the diagenetic sequences were concluded (Figure 4):

(1) Eodiagenetic stage A (late Triassic to early Jurassic)

In this stage, the basin subsided steadily, the maximum ground temperature was close to 60°C, and the burial

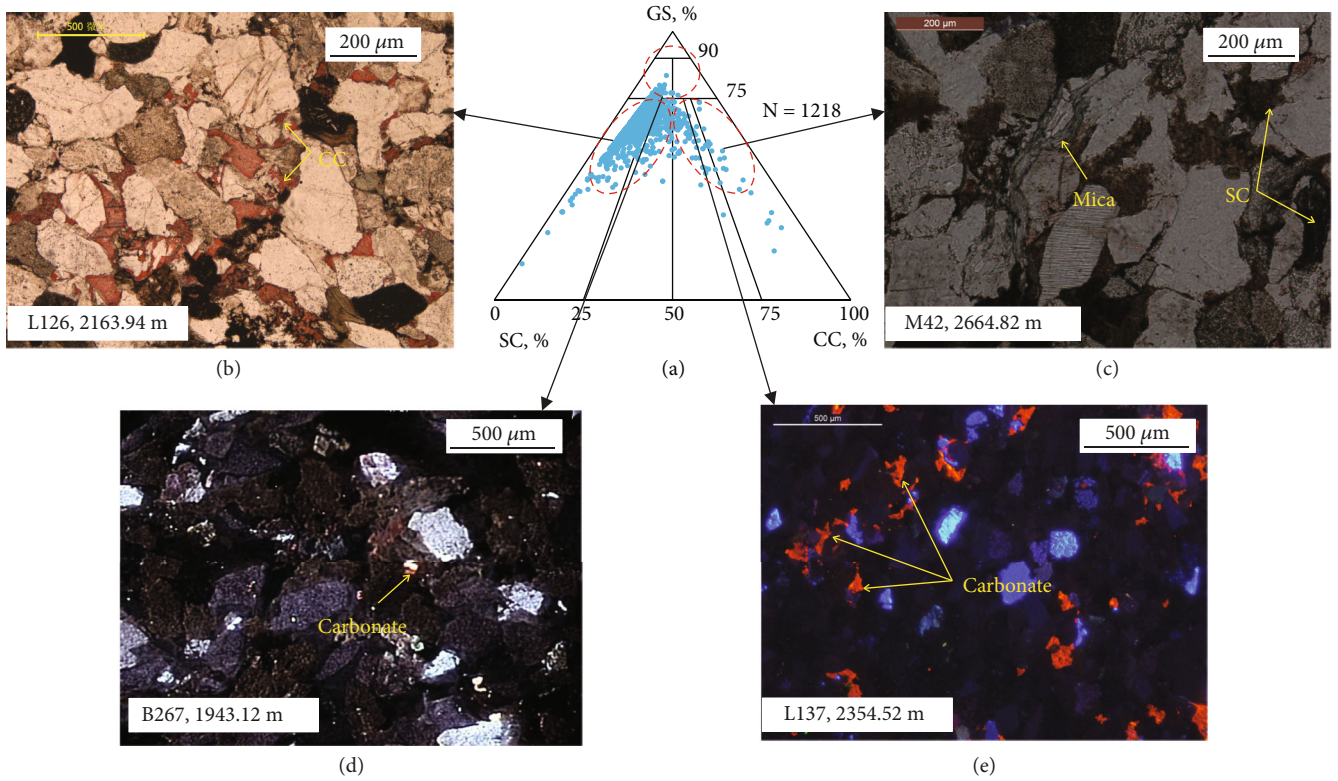

Figure 8: (a) Compositions of sandstones plotted on a ternary diagram based on new classification criterion; casting thin section of (b) high soft component sandstone, (c) calcareous sandstone, (d) low soft component sandstone with continual oil emplacement, and (e) low soft component sandstone with intermittent oil emplacement. CC: calcite cement; GS: grain skeleton; SC: soft component.

depth was less than 1100 m (Figure 12). The organic matter belonged to the early immature low mature stage. The decomposition of mica and igneous cuttings resulted in the alkalinity of the reservoir and the generation of magnesium, which led to the continuous precipitation of early pore-lining chlorite. At the same time, the alkaline environment made the carbonate materials in the pore fluid easier to precipitate, and the early carbonate cementation begins to form. With the increase of burial depth and the continuous compaction, the semidirectional arrangement of particles is prominent. The plastic clasts are pseudohybridized then fill the pores, destroying the primary pore space to a certain extent (Figure 4).

(2) Eodiagenetic stage B (early Jurassic to early Cretaceous)

In this stage, the basin subsided with fluctuations. The geothermal temperature hovered before 50-100°C, the maximum burial depth was close to 1800 m, and the organic matter was in the low maturity stage (Figure 12). Due to the overall subsidence of the stratum, compaction is dominant in this stage, the early coated chlorite continues to form, and the early siliceous and kaolinite begin to appear. At present, the hydrocarbon produced in this stage mainly occurs in carbonate and secondary quartz margin or pore-lining chlorite (Figures 4 and 12(b)).

(3) Mesodiagenetic stage A (early Cretaceous to middle-late Cretaceous)

In this stage, the basin is stable subsidence stage. The maximum burial depth is 2860 m, the ground temperature is over 130°C, and the organic matter is in a semimature stage. In this stage, kaolinite and siliceous cementation continued, while illite and late carbonate cementation began to form. The second and third stages of oil and gas charging all occur in this stage. The second stage of hydrocarbon charging mainly occurs in other secondary minerals, which exist in adsorbed hydrocarbons. The third stage of hydrocarbon charging is the most critical and most significant filling period of the target layer in the study area. According to the homogenization temperature of fluid inclusions, the second stage of hydrocarbon charging mainly occurs in other secondary minerals. The third stage of hydrocarbon charging is the most critical and most considerable filling period of the target layer in the study area. Most hydrocarbon charging occurs at this stage (Figures 9 and 12(b)). At the same time, due to a large amount of hydrocarbon filling, the organic-inorganic reaction in the target layer is active, and the acid fluid dissolves feldspar and other unstable minerals in the formation, formed dissolution pores [30]. With the dissolution of feldspar, kaolinite precipitates and filled the pore space. At the same time, due to the increased solubility of silica in the fluid, there is one-stage precipitation in the

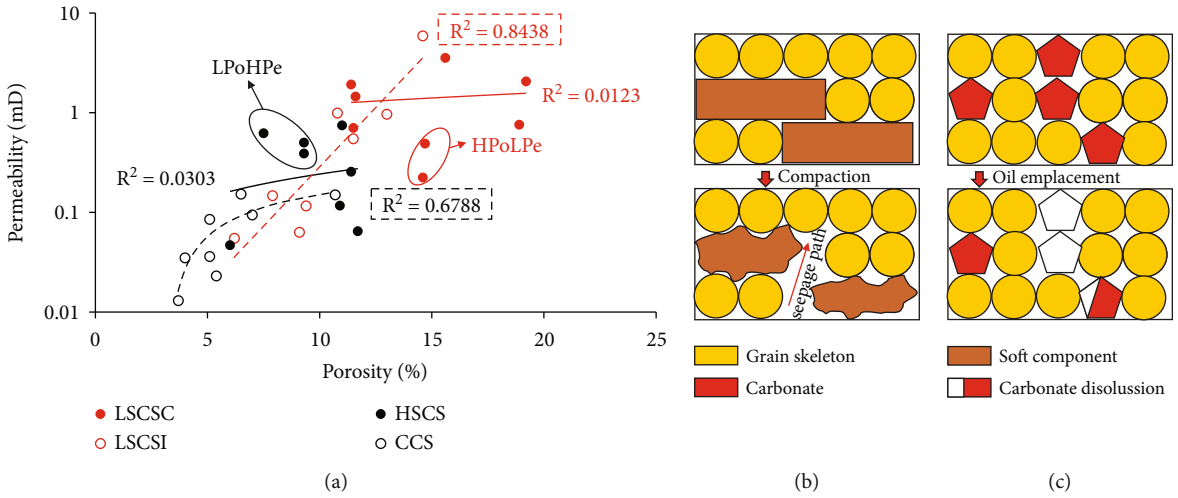

Figure 9: (a) The porosity against permeability; (b) schematic overview of compactional evolution for high soft component sandstones; (c) schematic overview of oil emplacement happened during diagenesis for low soft component sandstones with continual oil emplacement. LPoHPe: low porosity and high permeability samples; HPoLPe: high porosity and low permeability samples.

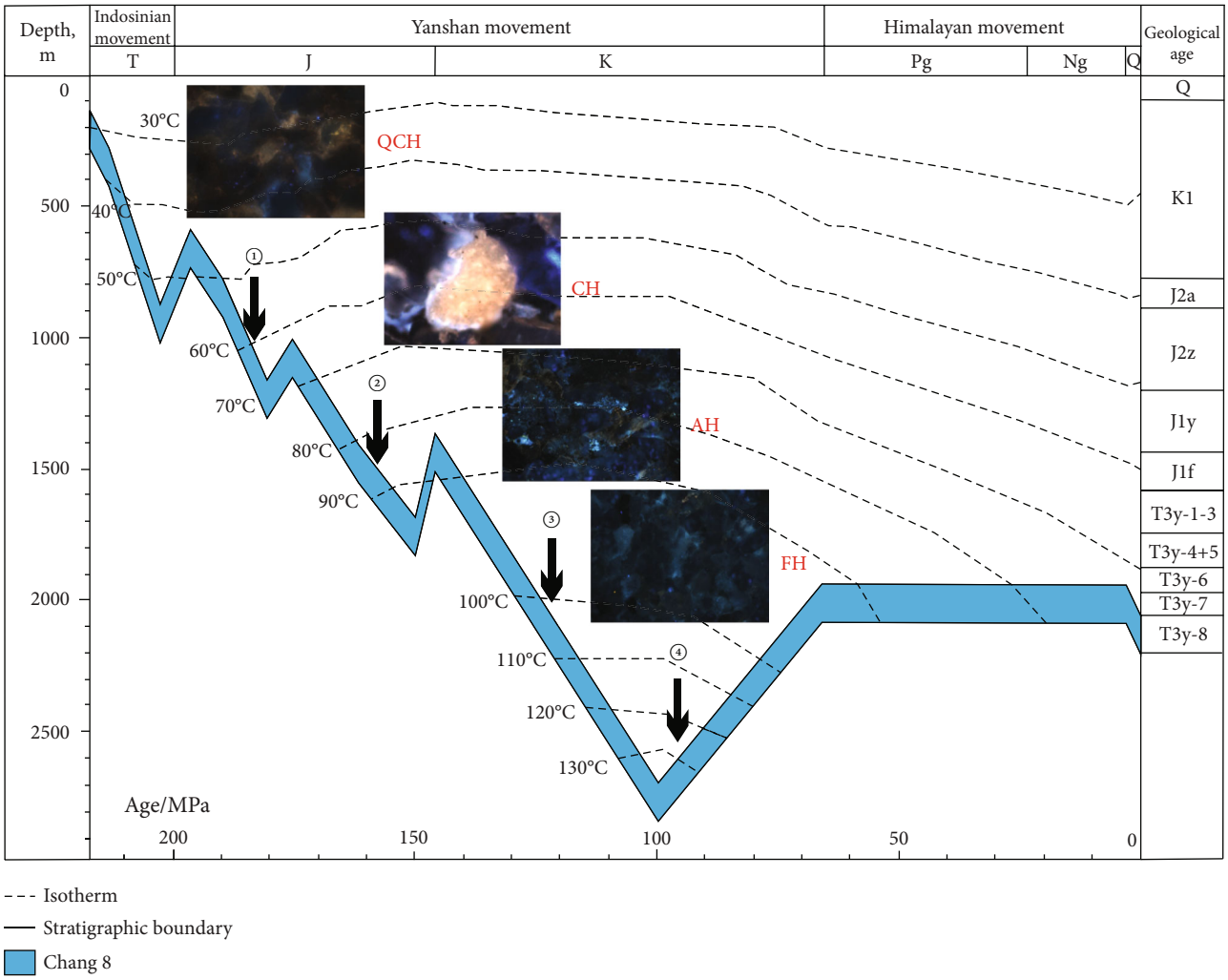

Figure 10: Burial, thermal, and oil emplacement history plots for the Chang 8 sandstone. QCH: quartz cement hydrocarbon; CH: carbonate hydrocarbon; AH: adsorbed hydrocarbon; FH: free hydrocarbon.

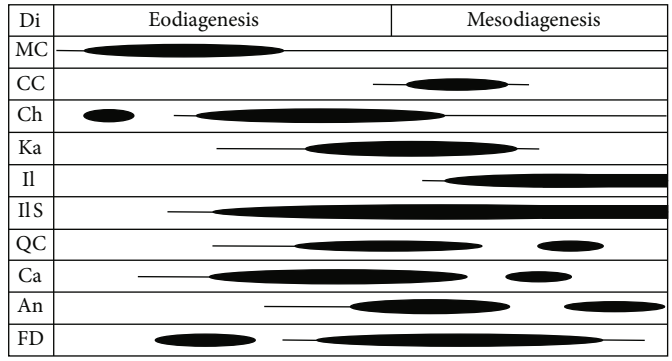

Figure 11: Diagenetic sequences of Chang 8 sandstone. MC: mechanical compaction; CC: chemical compaction; Ch: chlorite; Ka: kaolinite; Il: illite; I/S: illite smectite mixed layer; QC: quartz cement; Ca: carbonate; An: ankerite; FD: feldspar dissolution.

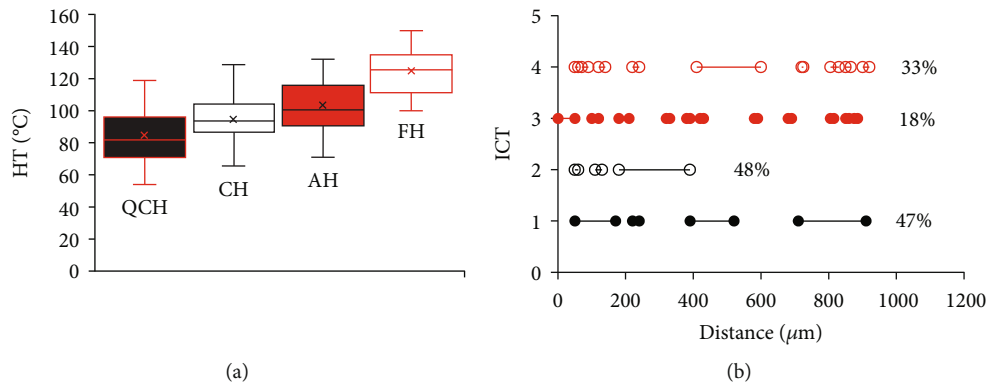

Figure 12: (a) Statistics of the homogenization temperatures of four types of hydrocarbons; (b) transverse distribution of coformed oil inclusions in or adjacent to minerals. (1) QCH: quartz cement hydrocarbon; (2) CH: carbonate hydrocarbon; (3) AH: adsorbed hydrocarbon; (4) FH: free hydrocarbon.

suitable environment, formed multistage siliceous cementation. At the same time, the burial depth and temperature of this stage are not ideal for transforming kaolinite to illite, resulting in the preservation of kaolinite (Figure 4).

(4) Mesodiagenetic stage B (late Cretaceous to present)

In this stage, the target form of the basin is in the overall trend of early tectonic uplift, medium-term basically stable and late slight decline, and finally formed the present reservoir appearance. At the same time, the diagenetic environment gradually changed from weak alkalinity to alkalinity due to the consumption of acidic media, resulting in a large number of illite, iron calcite, and iron dolomite cementation. The last stage of hydrocarbon charging occurred in this period, with a small scale and mainly in free and adsorbed states (Figures 4 and 12(b)).

4.5. Effects of Oil Emplacement and Diagenesis on Pore Network Evolution. In order to demonstrate the pore network evolution in geological time, the findings from Paxton and Houseknecht were used for paleo-porosity determination [24, 31, 32]. The lost porosity was mainly reflected in the content of intergranular pores, the cement development degree, and the matrix's development degree. Pore lining chlorite, calcite, etc. was belonged to early cementation minerals and led to pore reduction. Iron calcite, iron dolomite, illite, and other minerals usually belong to late cementation products, which also caused porosity loss.

Figure 13 illustrates the pore network evolution. We found that the initial porosity of different types of sandstones has similar values. The compaction stage showed that the high soft component sandstone is the most strongly modified by compaction. The calcareous cementation has relatively strong compaction resistance due to the almost total loss of intergranular pores. Late cementation generally destroys the pore spaces in the cementation stage, while early cementation often resists compaction. However, it should be pointed out that this result seems to be contradictory to the previous results: "in calcareous sandstones, the early cemented minerals generally belong to carbonate" because the early cemented loss porosity of calcareous sandstone is the least among the four types of sandstone. This is because it is generally considered that iron calcite and iron dolomite are late cementation products. At the same time, there are few early cementation products, such as calcite and dolomite, in the target layer in the study area, which evolved into late iron carbonate products. Therefore, the late

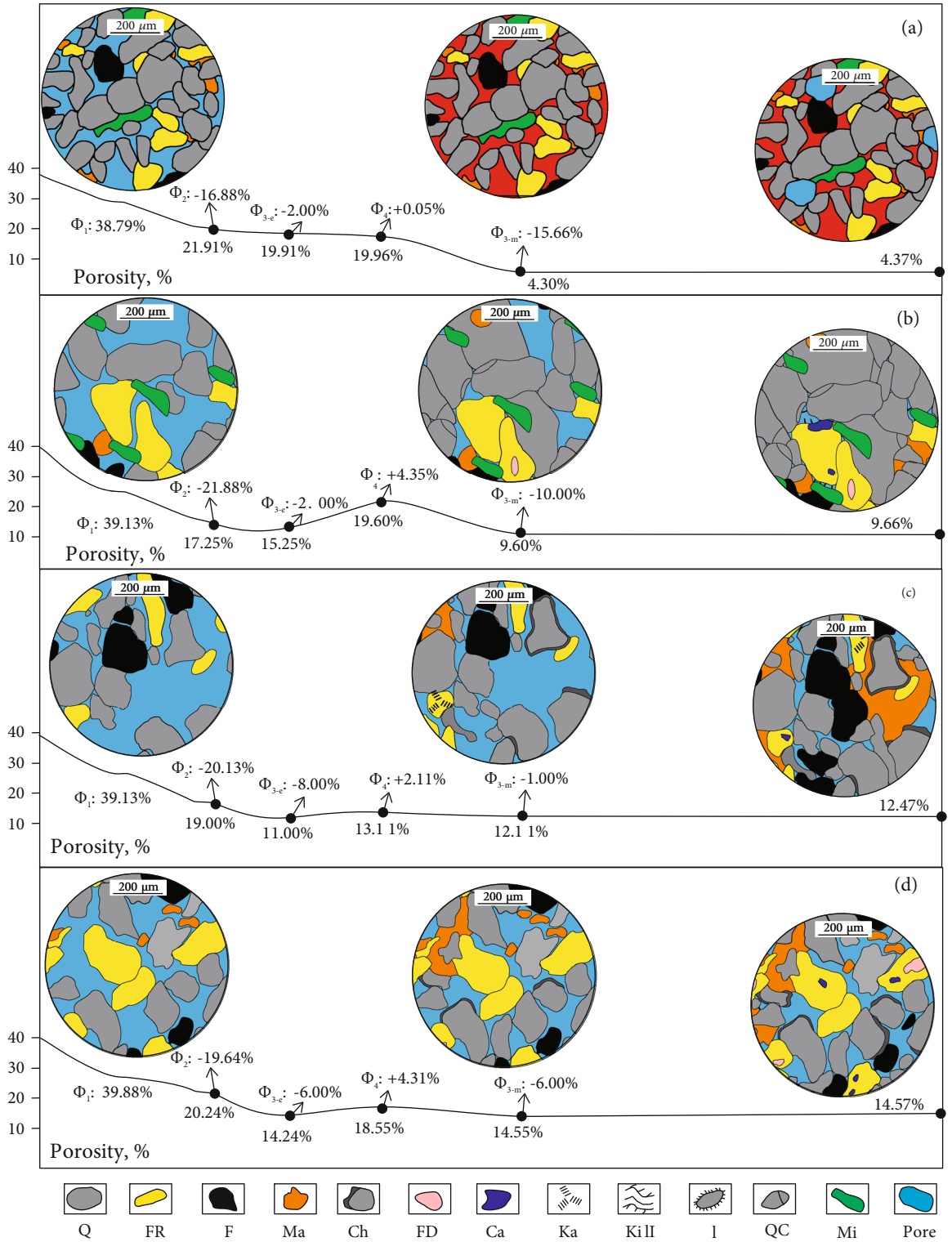

Figure 13: Pore evolution path for different types of sandstones. Q: quartz; F: feldspar; RF: rock fragment; Ma: matrix; Ch: chlorite; FD: feldspar dissolution; Ca: carbonate; Ka: kaolinite; Kil: kaolinite illitritization; Il: illite; QC: quartz cement; Mi: mica.

cementation products are calculated in the statistical process of cementation diagenesis. Dissolution could contribute to more pore spaces, especially for the low soft component sandstone with continual oil emplacement.

All in all, the above analysis demonstrated that oil emplacement is one of the crucial factors in pore network evolution. Based on the evolution path, the favorable zones could be determined: if a core belongs to low soft component

sandstone with continual oil emplacement, it is likely that this core corresponding to a high oil richness zone; if a core is filled with calcite, the possibility of effective reservoir becomes significantly less.

5. Conclusions

Establishing the link between oil emplacement with diagenetic sequences is crucial for understanding their controls on pore network evolution. This is exemplified by the tight sandstones of the Chang 8 Member of Upper Triassic Formation, Ordos Basin. This study found the following:

Four main lithofacies associations were identified based on new classification criteria: calcareous sandstone, high soft component sandstone, low soft component sandstone with continual oil emplacement, and low soft component sandstone with intermittent oil emplacement. Two of them have considerable physical properties heterogeneity.

The quartz cement-captured hydrocarbons have the lowest maturity and corresponding to primarily oil emplacement. The free hydrocarbons have the highest maturity, and they were the main contributors to the large-scale oil emplacement, which happened in the late Jurassic to early Cretaceous.

Diagenetic alterations of the Chang 8 tight sandstones have been achieved during eo- and meso diagenesis. Key diagenetic processes and alterations include mechanical compaction, formation of chlorite, illite, illite smectite mixed layer, and feldspar dissolution.

Calculation of porosity, consisting of diagenetic alterations and oil emplacement, has shown that mechanical compaction was the profound deterioration for all types of sandstones. Calcite would deteriorate the reservoirs for strong cementation. High soft components were easily compacted and led to low pore space. Macroporosity and permeability were preserved in the reservoirs due to continual oil emplacement.

Data Availability

The experimental data used to support the findings of this study are included within the manuscript.

Conflicts of Interest

The authors declare that there are no conflicts of interest regarding the publication of this paper.

Authors' Contributions

Huifang Hu contributed to the conceptualization, funding acquisition, and writing—original draft. Yang Ju contributed to the investigation, methodology, project administration, and supervision. Chenyang Zhao contributed to the funding acquisition and methodology. Miaozhi Jing contributed to the English editing and investigation. Liang Sun contributed to the figure drawing and data curation. Wei Sun contributed to the methodology and investigation. Dengke Liu contributed to the writing—review and editing. Lin Yang contributed to the investigation and data curation. Yue Jing contributed to the figure drawing and data curation. Guoqiang Huang contributed to the figure drawing, investigation, and methodology.

Acknowledgments

This work was supported by the National Natural Science Foundation of China (12072256), the Shaanxi research and development program (2021GY-113), and the Basic research program of Natural Science in Shaanxi Province (2019JQ-151, 2021JQ-029, 2021JM-543, 2021JM-406).

Supplementary Materials

Supplementary material contained Table S1 to Table S4, which showed the parameters derived from physical properties, XRD, geochemical analysis, and cooling-heating stages. *(Supplementary Materials)*

References

[1] C. Zou, Z. Yang, S. Tao et al., "Continuous hydrocarbon accumulation over a large area as a distinguishing characteristic of unconventional petroleum: the Ordos Basin, North-Central China," *North-Central China. Earth-Science Reviews*, vol. 126, pp. 358–369, 2013.

[2] W. Qi, X. Yun, W. Xiaoquan, W. Tengfei, and S. Zhang, "Volume fracturing technology of unconventional reservoirs: connotation, design optimization and implementation," *Petroleum Exploration and Development*, vol. 39, no. 3, pp. 377–384, 2012.

[3] Q. Tan, Y. Kang, L. You, F. Xu, and S. Meng, "A comprehensive insight into the multiscale pore structure characterization of saline-lacustrine tight carbonate reservoir," *Journal of Petroleum Science and Engineering*, vol. 187, article 106744, 2020.

[4] R. Rezaee, A. Saeedi, and B. Clennell, "Tight gas sands permeability estimation from mercury injection capillary pressure and nuclear magnetic resonance data," *Journal of Petroleum Science and Engineering*, vol. 88-89, pp. 92–99, 2012.

[5] T. Ramstad, N. Idowu, C. Nardi, and P.-E. Øren, "Relative permeability calculations from two-phase flow simulations directly on digital images of porous rocks," *Transport in Porous Media*, vol. 94, no. 2, pp. 487–504, 2012.

[6] S. Zendehboudi and A. Bahadori, *Shale Oil and Gas Handbook: Theory, Technologies, and Challenges*, Gulf Professional Publishing, 2017.

[7] R. G. Loucks, R. M. Reed, S. C. Ruppel, and U. Hammes, "Spectrum of pore types and networks in mudrocks and a descriptive classification for matrix-related mudrock pores," *AAPG Bulletin*, vol. 96, no. 6, pp. 1071–1098, 2012.

[8] J. Lai, G. Wang, Y. Ran, Z. Zhou, and Y. Cui, "Impact of diagenesis on the reservoir quality of tight oil sandstones: the case of Upper Triassic Yanchang Formation Chang 7 oil layers in Ordos Basin, China," *Journal of Petroleum Science and Engineering*, vol. 145, pp. 54–65, 2016.

[9] X. Shao, X. Pang, F. Jiang, L. Li, Y. Huyan, and D. Zheng, "Reservoir characterization of tight sandstones using nuclear magnetic resonance and incremental pressure mercury injection experiments: implication for tight sand gas reservoir quality," *Energy & Fuels*, vol. 31, no. 10, pp. 10420–10431, 2017.

[10] J. Lai, G. Wang, Z. Wang et al., "A review on pore structure characterization in tight sandstones," *Earth-Science Reviews*, vol. 177, pp. 436–457, 2018.

[11] J. Qiao, J. Zeng, S. Jiang, and Y. Wang, "Impacts of sedimentology and diagenesis on pore structure and reservoir quality in tight oil sandstone reservoirs: implications for macroscopic and microscopic heterogeneities," *Marine and Petroleum Geology*, vol. 111, pp. 279–300, 2020.

[12] H. Zhu, Y. Ju, Y. Qi, C. Huang, and L. Zhang, "Impact of tectonism on pore type and pore structure evolution in organic-rich shale: implications for gas storage and migration pathways in naturally deformed rocks," *Fuel*, vol. 228, pp. 272–289, 2018.

[13] E. de Boever, C. Varloteaux, F. H. Nader et al., "Quantification and prediction of the 3D pore network evolution in carbonate reservoir rocks," *Oil & Gas Science and Technology–Revue d'IFP Energies Nouvelles*, vol. 67, no. 1, pp. 161–178, 2012.

[14] L. Wang, W.-X. Tian, X.-Y. Zhao, and C.-Q. Huang, "Numerical simulation of the effects of canopy properties on airflow and pollutant dispersion in street canyons," *Indoor and Built Environment*, 2021.

[15] S. Ehrenberg, "Relationship between diagenesis and reservoir quality in sandstones of the Garn Formation, Haltenbanken, mid-Norwegian continental shelf," *AAPG Bulletin*, vol. 74, no. 10, pp. 1538–1558, 1990.

[16] S. Morad, K. Al-Ramadan, J. M. Ketzer, and L. De Ros, "The impact of diagenesis on the heterogeneity of sandstone reservoirs: a review of the role of depositional facies and sequence stratigraphy," *AAPG Bulletin*, vol. 94, no. 8, pp. 1267–1309, 2010.

[17] G. Wang, X. Chang, W. Yin, Y. Li, and T. Song, "Impact of diagenesis on reservoir quality and heterogeneity of the Upper Triassic Chang 8 tight oil sandstones in the Zhenjing area, Ordos Basin, China," *China. Marine and Petroleum Geology*, vol. 83, pp. 84–96, 2017.

[18] A. Q. Raeini, B. Bijeljic, and M. J. Blunt, "Modelling capillary trapping using finite-volume simulation of two-phase flow directly on micro-CT images," *Advances in Water Resources*, vol. 83, pp. 102–110, 2015.

[19] R. Worden and S. Morad, *Clay Minerals in Sandstones: Controls on Formation, Distribution and Evolution*, vol. 34, Special Publication-International Association of Sedimentologists, 2003.

[20] S. Sathar, R. H. Worden, D. R. Faulkner, and P. C. Smalley, "The effect of oil saturation on the mechanism of compaction in granular materials: higher oil saturations lead to more grain fracturing and less pressure solution," *Journal of Sedimentary Research*, vol. 82, no. 8, pp. 571–584, 2012.

[21] Z. Wenzhi, W. Hongjun, X. Chunchun, B. Congsheng, W. Zecheng, and G. Xiaohui, "Reservoir-forming mechanism and enrichment conditions of the extensive Xujiahe Formation gas reservoirs, central Sichuan Basin," *Petroleum Exploration and Development*, vol. 37, no. 2, pp. 146–157, 2010.

[22] D. Liu, J. Su, Z. Gu et al., "Geochemical properties and pore structure control on oil extraction of shale," *Lithosphere*, vol. 2021, no. Special 1, article 6646791, 2021.

[23] J. Yan, X. He, S. Zhang et al., "Sensitive parameters of NMR T_2 spectrum and their application to pore structure characterization and evaluation in logging profile: a case study from Chang 7 in the Yanchang Formation, Heshui area, Ordos Basin, NW China," *Marine and Petroleum Geology*, vol. 111, pp. 230–239, 2020.

[24] B. Bai, R. Zhu, S. Wu et al., "Multi-scale method of Nano(Micro)-CT study on microscopic pore structure of tight sandstone of Yanchang Formation, Ordos Basin," *Ordos Basin. Petroleum Exploration and Development*, vol. 40, no. 3, pp. 354–358, 2013.

[25] R. Worden and S. Barclay, "The effect of oil emplacement on diagenetic clay mineralogy: the Upper Jurassic Magnus Sandstone Member, North Sea," in *Clay Mineral Cements in Sandstones*, pp. 453–469, Wiley, 1999.

[26] S. Zendehboudi, I. Chatzis, A. A. Mohsenipour, and A. Elkamel, "Dimensional analysis and scale-up of immiscible two-phase flow displacement in fractured porous media under controlled gravity drainage," *Energy & Fuels*, vol. 25, no. 4, pp. 1731–1750, 2011.

[27] M. Schmitt, C. P. Fernandes, F. G. Wolf, J. A. B. da Cunha Neto, C. P. Rahner, and V. S. S. dos Santos, "Characterization of Brazilian tight gas sandstones relating permeability and Angstrom-to micron-scale pore structures," *Journal of Natural Gas Science and Engineering*, vol. 27, pp. 785–807, 2015.

[28] R. L. Folk, *Petrology of Sedimentary Rocks*, Hemphill publishing company, 1980.

[29] L. M. Anovitz and D. R. Cole, "Characterization and analysis of porosity and pore structures," *Reviews in Mineralogy and Geochemistry*, vol. 80, no. 1, pp. 61–164, 2015.

[30] D. Liu, D. Ren, K. Du, Y. Qi, and F. Ye, "Impacts of mineral composition and pore structure on spontaneous imbibition in tight sandstone," *Journal of Petroleum Science and Engineering*, vol. 201, article 108397, 2021.

[31] P. Paxton, "Social capital and democracy: an interdependent relationship," *American Sociological Review*, vol. 67, no. 2, p. 254, 2002.

[32] D. W. Houseknecht, "Assessing the relative importance of compaction processes and cementation to reduction of porosity in sandstones," *AAPG Bulletin*, vol. 71, no. 6, pp. 633–642, 1987.